Impact safety improvement of high explosives through the use of internal cavity design

Zhaofei Xiao[a], Ryan Thornhill[a], Hari Arora[b], Robert Warren[a], and Fawzi Belblidia[a]

[a] ASTUTE EAST, College of Engineering, Swansea University, Swansea, UK, SA1 8EN

[b] Faculty of Science and Engineering, Swansea University, Swansea, UK, SA1 8EN

Key words: High explosive, blast, safety, additive manufacturing

Abstract

This study offers improved safety design guidelines for high explosives (HE), creating impact insensitive geometries, capitalising on the potential for additive layer manufacturing techniques. There are numerous safety concerns when considering energetic materials and HEs, the primary concern, subject of this work, is the risk of unplanned detonation from impact. There are multiple potential causes for unplanned detonation due to impact; one of which is the impact from a high-speed foreign object. Despite this substantial risk, the problem has not been publicly addressed by means of adjusting the design of the charge itself. Therefore, investigations into the internal design of the charge were executed, whereby the inclusion of various sized and shaped voids are assessed, to establish their effect upon the reactivity of the HE. Using computational modelling, allows for numerous designs to be assessed and developed, and the impact sensitivity of the charge to be tested across a range of scenarios. The proposed validated computational model enables designs to be optimised in a safe and efficient manner, reducing the number of physical tests required, and thus minimising time, cost and the environmental impact.

Introduction

Explosives are often used for military, mining, and construction purposes. They are typically made up of a casing, housing an explosive chemical compound, with a fuse or detonation system. With the most common geometries of explosives, being solid cylinders, cubes, and cuboids. The explosive chemical compound is usually triggered by heat, shock, friction, or a combination of these. This in turn results in a rapid release of heat and high-pressure gasses, which expand rapidly overcoming its confines [1]. This rapid release of energy results in fragmentation of the casing and confining structures, and a blast of air that causes loose debris to be expelled from the explosion site, and ground vibration.

One primary purpose of accurate modelling of HEs is to understand the blast effect on surrounding items and structures, and to utilise the information to better design safety equipment against such blasts. For example, Makwana et al [2] investigated the structural rigidity improvement of armoured vehicles against anti-vehicle mine blasts, and the study from Rasico [3] highlights the importance of capturing the fragmentation of explosive casings, as these can often have the ability to pierce protective armour.

Normally, the detonation of explosives is carefully planned and executed to achieve the desired explosion results. However, there is a significant risk posed by unplanned detonations of high explosives. For example, an unintentional impact force may be applied on the charge during the manufacturing, transit, or storage processes. In order to improve the safety performance of explosives under unexpected impact, this paper promotes a novel concept using HEs with tailored internal hollow sections, to reduce the reactivity of the charge to prevent unplanned detonations, while allowing for the HEs to achieve their target blast performance. In addition, this concept can also eliminate the impact on explosives use costs, because the existing casing and transportation setups for explosives do not need to be modified for the purpose of increasing safety.

To enable the internal designs to be considered, a practical manufacturing method must be known. Therefore, additive layer manufacturing (ALM) is suggested as the most prudent method, to allow for the inclusion of internal voids of desirable sizes and for much greater design scope for experiments and trials. ALM processes can easily generate geometrically complex shapes directly from computer models with little waste material. Currently, a casting/moulding process is used, which also offers the potential for the creation of enclosed internal geometries. However, due to the viscous nature of the energetic material it would be difficult to successfully fill the mould under normal conditions, with the additional pressure or heat input required, posing a safety concern. According to recent studies [4, 5], material extrusion ALM methods are a feasible manufacturing process for explosives. This paper solely focusses upon the explosive geometry design and consequent blast behaviour, due to the limited access to the flow properties of the energetic material during the ALM process.

Background and Method

Within the pre-existing publications, several methods for modelling blasts have been used, ranging from analytical [2], particle-based methods [6], mesh free [7] and coupled methods [8]. A common approach to predict the blast load of explosives, is the empirical CONWEP blast model [9]. However, it does not suit the scope of the present paper, as it only applies on spherical explosives and uses empirical formulae to generate spherical blast wave fronts. Two more suitable frequently cited methods are the pure lagrangian and Multi Material Arbitrary Lagrangian-~~Eularian~~ Eulerian (MM-ALE). To be able to investigate the blast behaviour of explosives in various shapes, the MM-ALE approach is widely used [10-12]. The MM-ALE approach offers accurate simulation results of explosion and fluid-structure interactions, as this approach allows each mesh to contain two or more materials and move independently with material flow, which overcomes severe element distortions [10, 13, 14]. Additional benefits of the MM-ALE method include the ability to capture shadowing (a feature of blast waves after interacting with objects, preventing the propagation of the blast wave) and the focusing of the blast wave, which is imperative when required to consider surrounding structures. However, MM-ALE often requires a higher level of computational intensity when compared to other options.

Within the MM-ALE method, a key controlling element of the model performance is the Equation of State (EOS) utilised to characterise the HE and the consequent blast. The EOS governs the pressure, energy, and density, and plays an essential role in explosive detonation simulation. Jones–Wilkins–Lee (JWL) EOS [15] is a typical EOS that is widely used, and has shown successful results when implemented in previous studies [10, 11]. The general form of the JWL EOS is presented in Equation (1).

$$P = Ae^{-R_1 V} + Be^{-R_2 V} + \omega C_v \frac{T}{V} \tag{1}$$

Where P is pressure, V is the relative volume, T is temperature, ω is Gruneisen coefficient, C_v is average heat capacity and A, B, R_1 and R_2 are calibration constants.

However, a more suitable version can be used when focusing on the internal detonation process and charges that are sometimes only partially detonated. This is the Ignition and Growth (I&G) EOS [16, 17], which contains the two forms of the basic JWL EOS; one for the reacted explosive and another for the unreacted portion, as well as a reaction rate law. The rate law is split into three sections, each utilised for different values of the reacted fraction. Each part describes the stages of reaction typically observed within the shock, initiation, and detonation of a heterogeneous solid explosive. The three parts are identified in Equation (2), where t is time, $\rho\cancel{F}$ is current density, $\rho\cancel{F}_{0\cancel{e}}$ is initial density and I, G1, G2, a, b, c, d, e, g, x, y `and z are empirically derived calibration constants [16]. The I&G EOS is applied in many successful cases on simulating detonation progress of solid explosives under impact [18-20].

$$\frac{dF}{dt} = I[1-F]^b\left[\frac{\rho}{\rho_0}-1-a\right]^x + G_1[1-F]^c\,F^dP^y + G_2[1-F]^e\,F^gP^z \qquad (2)$$

$$\{0 < F < F_{ig\,max}\} \qquad \{0 < F < F_{G1\,max}\} \quad \{F_{G2\,max} < F < 1\}$$

Validation

The proposed computational model was conducted under the commercial Finite Element Analysis software, LS-DYNA [21]. The MM-ALE method with I&G EOS was selected. In order to ensure the computational model used here is robust and reliable, a numerical validation work using both 2D and 3D models was carried out by reproducing the simulation model published in [22]. In this model, a cylindrical explosive with an aluminium plate located on the bottom face of the charge is used, with a projectile impacting this face, as displayed in

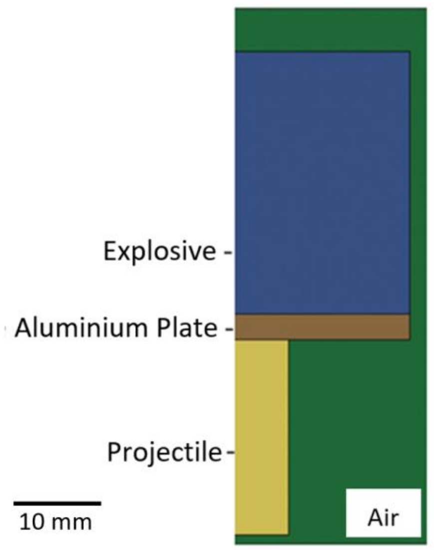

Figure 1~~Figure 1~~. The detailed material models and setups were taken from [22], and were reiterated in this paper for the sake of completeness.

Table 1~~Table 1~~ summarises the detonation impact speeds from the experimental and simulation data in [22] and the results of this validation work. It can be seen that the results of both the 2D and 3D models considered in this paper only have a difference of 1.2 % and are close to the experimental result reported in [22]. According to Figure 2~~Figure 2~~, the predicted morphologies of explosive after detonation from the 2D and 3D models are similar to the simulation results in [22]. Therefore, the proposed computational model offers reliable investigation results.

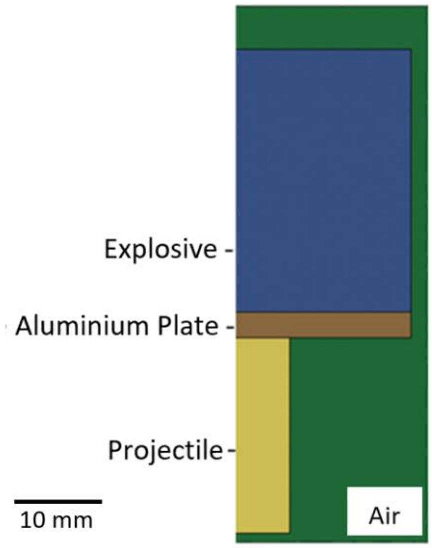

Figure 1 Schematic of axis symmetric 2D model used for validation

Table 1 The detonation impact speeds of the explosives reported in [22] and predicted by the 2D and 3D models using MM-ALE and I&G EOS approach in this paper

	Experimental data in [22]	2D model in [22]	2D model	3D model
Impact speed	1220 m/s	1165 m/s	1270 m/s	1255 m/s
Difference	-	-4.5 %	+4.1 %	+2.9 %

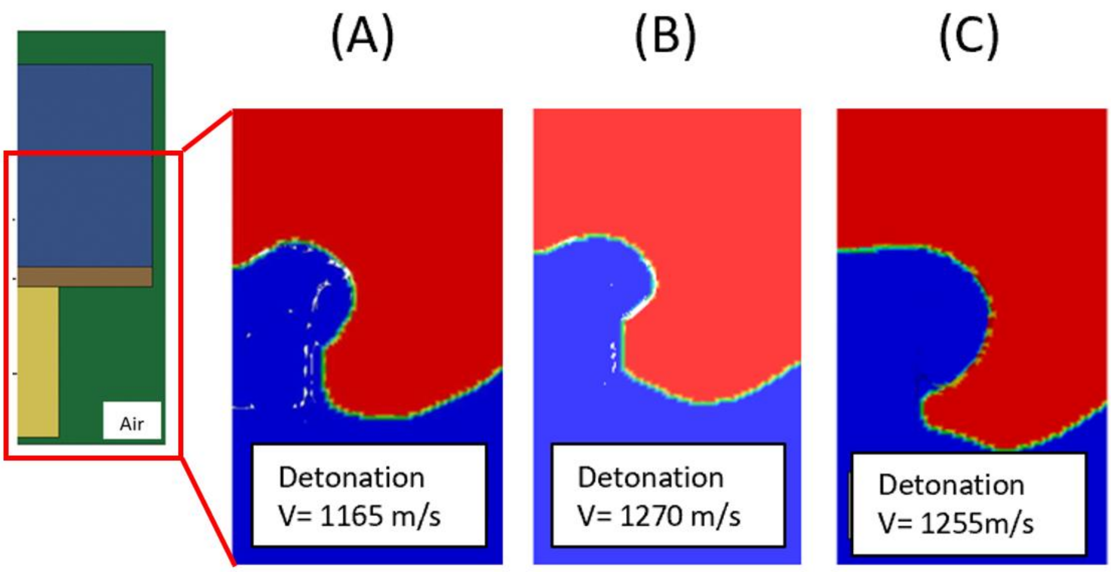

Figure 2 Comparison of shapes of detonated explosives (A) 2D result (mesh size 0.333 mm) reported in [22] (B) 2D (mesh size 0.25 mm) and (C) 3D model (mesh size 0.25 mm) in present work.

Proof of concept: Improve explosive safety via 2D simulation

A 2D axisymmetric model was initially created to prove the concept of improving the safety of explosive material by utilising internal hollow sections, while retaining comparable blast performance against equivalent solid explosives. The effects of the sizes and locations of the hollow sections on the blast behaviours were investigated. At later stage of this study, various 3D models using refined designs were considered to derive improved design safety guidelines.

In this paper, COMP-B was selected as a representative explosive material to investigate by using the I&G approach. In the simulations, a cylindrical explosive of 100 mm diameter and 100 mm length was impacted by a 50-gram brass projectile with a length of 49.5 mm and diameter of 12.7 mm in an ambient environment. This set up was selected based upon several established impact test procedures, such as Standardisation Agreement (STANAG) 4496, STANAG 4241 and Energetic Material Hazard Party (EMPTAP) test 36, whereby projectiles ranging from 13.5 grams to 250 grams are fired at speeds of up to 2530 m/s. With the utilised 50g projectile selected offering sufficient mass to trigger a detonation at speeds within the top end of these specifications.

Figure 3~~Figure 3~~ shows the setup of the 2D axisymmetric model. All the material models and associated parameters of the projectile and COMP-B are listed in Table 2~~Table 2~~. The projectile speed is then increased by an increment of 10 m/s and the safety performance of the explosive is assessed by the impact speed which can detonate the explosive material. The blast performance of the charge is evaluated by the pressures acquired at Sensors A and B (indicated in Figure 3~~Figure 3~~) once the explosive is fully detonated. Sensor A is located at the mid-point of the explosive, and is 25 mm far to the side surface, while Senor B is on the centre axis of the explosive and is 25 mm above the top surface.

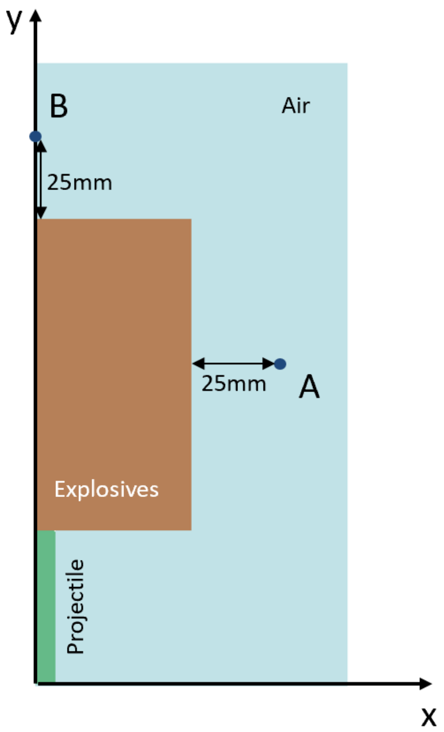

Figure 3 Schematics of the 2D axisymmetric model setups

Table 2 Parameters of the material models and EOS used in this paper taken from [22]

Component			**Parameters**	
COMP-B	Material Model	Elastic Plastic	ρ: 1717 kg/m^3; G_{shear}: 3.54 GPa; S_{yield}: 20 MPa	
	EOS	Ignition & Growth	Unreacted JWL	A: 4.85×10^{13} Pa; B: -3.9×10^9 Pa; R_1: 11.3; R_2: 1.13; ω: 0.8938; C_v: 2.487×10^6 Pa/K; T_0: 298 K.
			Reacted JWL	A: 5.242×10^{11} Pa; B: 7.678×10^9 Pa; R_1: 4.2; R_2: 1.11; ω: 0.5; C_v: 1.0×10^6 Pa/K; E_0: 8.5×10^9 Pa.
			Reaction rate	a: 0.0367; b: 0.667; c: 0.667; d: 0.333; e: 0.222; g: 1; x: 7; y: 2; z: 3; F_{G1max}: 0.7; F_{G2min} = 0; I: 4×10^7 s^{-1}; G_1: 1.4×10^{-14} Pa^{-1}S^{-1}; G_2: 1.0×10^{-24} Pa^{-1}S^{-1}.
Projectile	Material Model	Elastic Plastic	ρ: 8020 kg/m^3; G_{shear}: 81.0 GPa; S_{yield}: 1375 MPa	
	EOS	Gruneisen	C: 4569; S_1: 1.49; S_2: 0; S_3: 0; $γ_0$: 2.17 ; α: 0.46	
Air	Material Model	Null	ρ: 1.225 kg/m^3	
	EOS	Linear Polynomial	C_0: 0; C_1: 0; C_2: 0; C_3: 0; C_4: 0.4; C_5: 0.4; C_6: 0; E_0: 2.5 × 10^5; V_0: 1	

In terms of the internal voids in the 2D explosive model for improving safety, their cross-sectional shape was designed to be ~~spherical~~ circle with two sizes selected to investigate (3 mm and 6 mm in radius). The explosive designs in the 2D axisymmetric model are schematically shown in Figure 4~~Figure 4~~. The explosives with the small and large hollow sections have the same cavity volume fraction (6.5 vol. %). Hence, the equivalent solid explosive is 93.5 mm long to ensure all of the explosive charges contain the same amount of energetic material. In addition, the effects of the hollow section location were investigated, by examining two distances between the bottom surfaces of the hollow sections and the leading edge of the explosive (5 mm and 10 mm were selected and shown as d in Figure 4~~Figure 4~~).

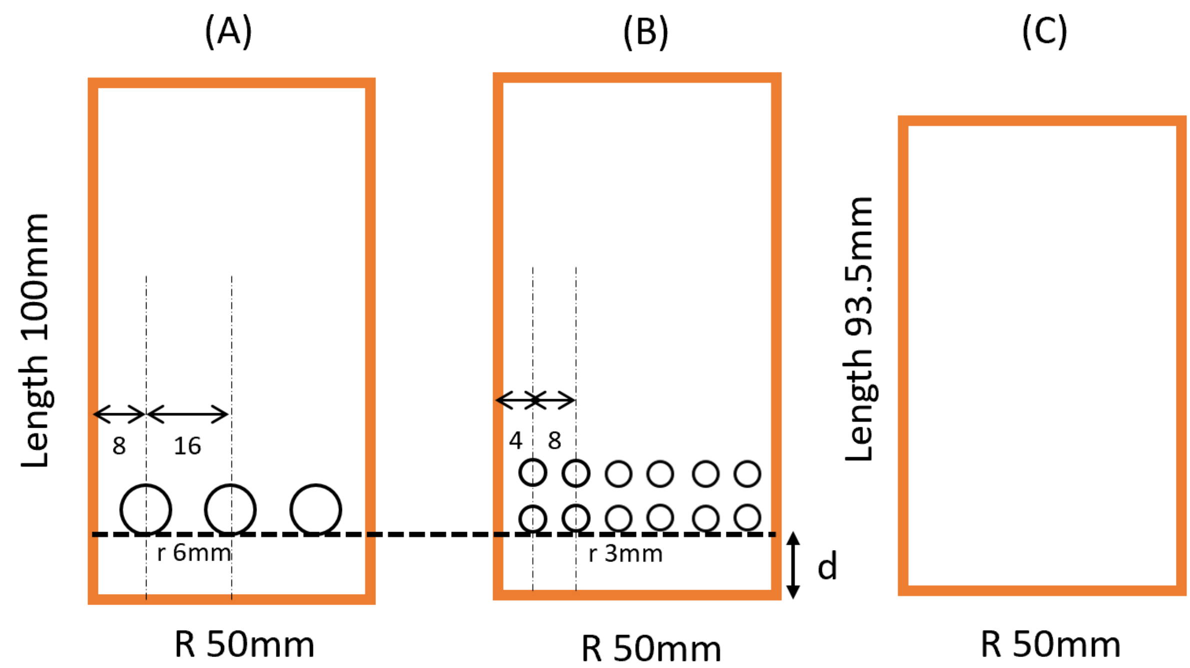

Figure 4 Schematics of explosives with (A) large (r=6 mm) and (B) small (r=3 mm) hollow sections and (C) the equivalent solid explosive

After a mesh sensitivity study where the accuracy of simulation results of blast wave pressure and computational cost was weighted, the element size was selected as 0.25 mm in the structured mesh. Similar mesh sensitivity study results can be found in [22].

Table 3~~Table 3~~ lists the detonation impact speed of all the investigated explosives, with and without the internal hollow voids. It can be seen that the presence of the internal hollow section improves the detonation impact speed, when compared to the equivalent solid explosive, which can be detonated at the impact speed of 1040 m/s. However, the improvement is only around 2 % when the hollow sections are 10 mm away from the bottom impact surface of the explosives, no matter what the size of hollow sections. When the hollow sections are located at only 5 mm above the bottom surface, the improvement in detonation impact speed becomes more significant. The small hollow sections provide an improvement of 34.6 % in the detonation impact speed, compared to the speed of the solid explosive, while the large hollow sections result in an increase in speed of 76.9 % to 1840 m/s.

Table 3 The detonation impact speed of the solid explosives and the explosives with small and large hollow sections in the 2D axisymmetric model

Location of the hollow sections	Solid explosive	Explosive with small hollow section	Explosive with large hollow section
d = 5 mm	1040 m/s	1400 m/s (+34.6%)	1840 m/s (+76.9%)
d = 10 mm		1060 m/s (+1.9%)	1060 m/s (+1.9%)

Figure 5~~Figure 5~~ shows the burn fraction over series of time steps of the explosives with and without the internal hollow sections, when impacted by their detonation speeds listed in Table 3~~Table 3~~. It can be seen that the detonation progression of all the explosives are different. (B) and (C) in Figure 5~~Figure 5~~, for the explosives with the hollow sections 10 mm away from the impact surface, shows once the explosive materials near the projectile are detonated at the initial stage (< 3 μs) like the solid explosive, there is sufficient energetic material within that 10 mm region to support the detonation progressing continuously until the whole charge is fully detonated. Hence, their detonation speeds are close with each other. Although whilst these two types of explosives cannot provide significant improvement in impact safety, it is worth noting that the large hollow sections create a more flattened blast front. The detailed study on tailoring blast fronts through the use of voids will be discussed in future publications.

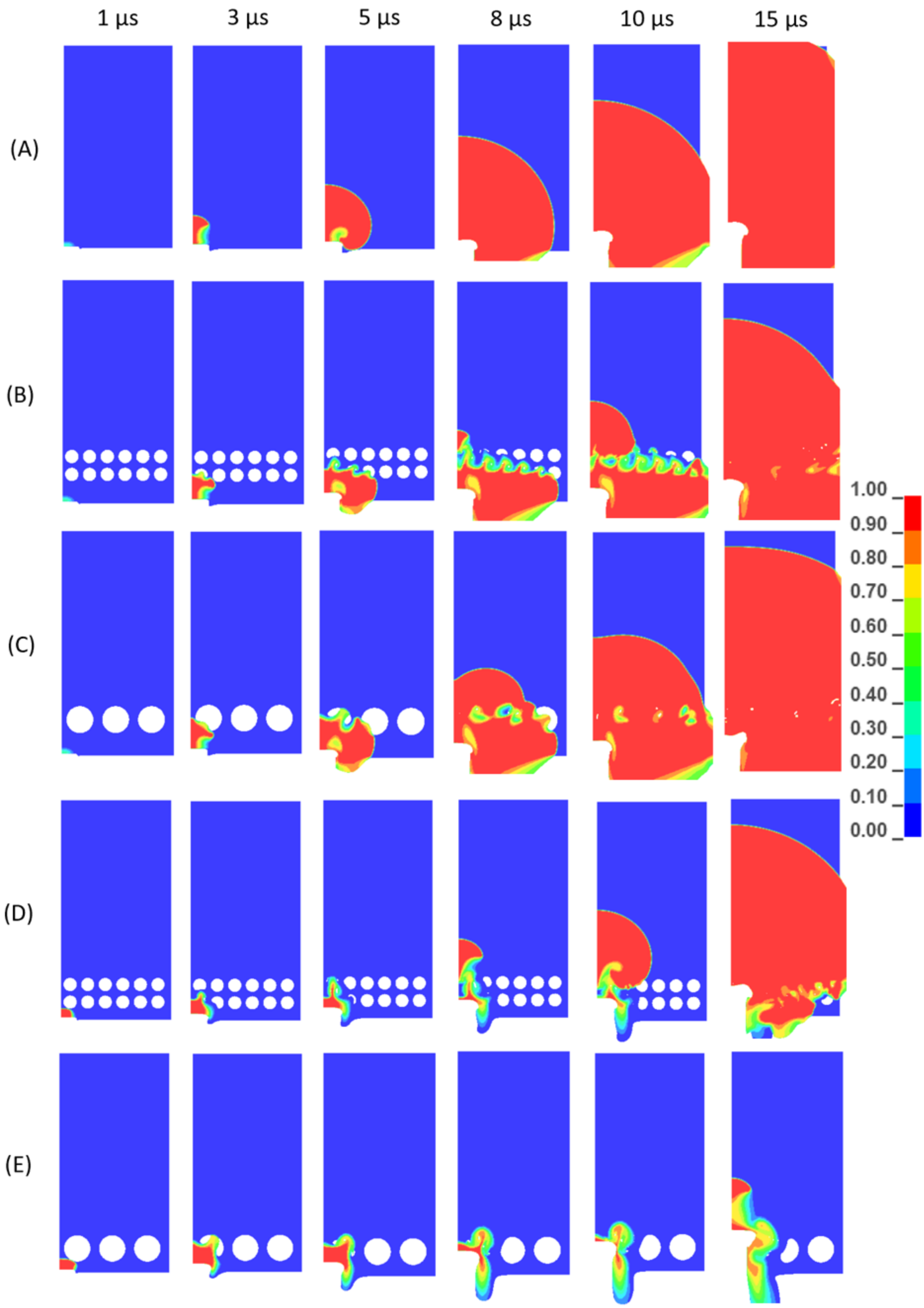

Figure 5 Burn fraction contour plots at different time stages of all the investigated explosives in the 2D axisymmetric models: (A) Solid explosive; (B) Explosive with small hollow sections (d = 10 mm); (C) Explosive with large hollow sections (d = 10 mm); (D) Explosive with small hollow sections (d = 5 mm); (E) Explosive with large hollow sections (d = 5 mm), note that this explosive continued to burn completely after 15 μs.

When the hollow sections are closer to the impact surface (d = 5 mm), the severe detonation is delayed to approximate 8 µs by the small voids (at impact speed of 1400 m/s) and to 15 µs by the large voids (at impact speed of 1840 m/s), as shown in Figure 5~~Figure 5~~ (D) and (E). This can be ascribed to larger pressure dissipation capacity from the large hollow sections. According to Figure 6~~Figure 6~~, the initial maximum pressure of 31 GPa is reduced to 2.4 GPa by the small voids at 3.6 µs, whilst the large voids can decrease the pressure to 1.8 GPa even under a higher impact speed from projectile (1840 m/s (+76.9%)).

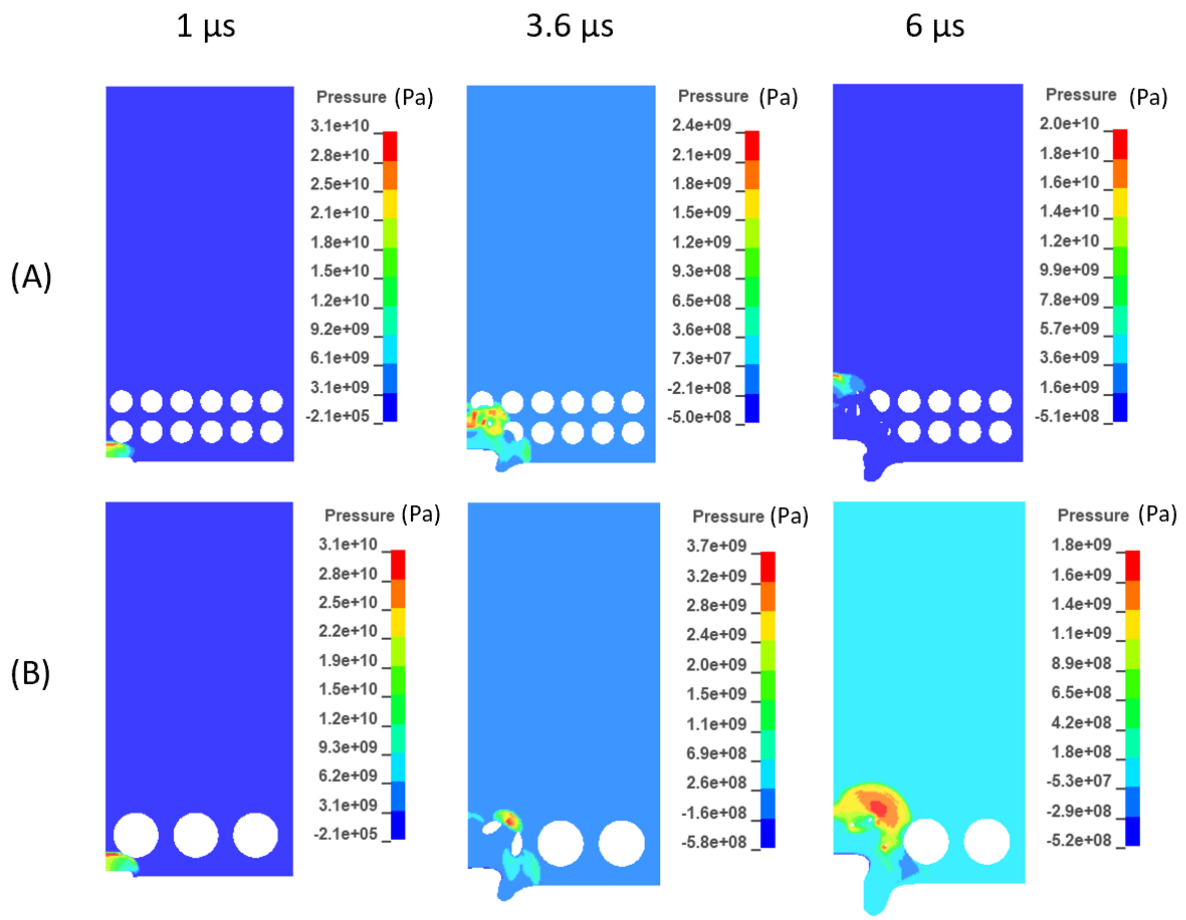

Figure 6 Blast pressure in the explosives with (A) small and (B) large hollow sections

Table 4~~Table 4~~ lists the maximum pressure and arrival time at sensors A and B for the solid explosive and the explosives with hollow sections set 5mm from the impact site. It can be seen that all three types of explosives generate a similar level of blast pressure, but by increasing the size of the hollow sections, the blast wave arrival time is postponed due to the delayed detonation as illustrated in Figure 5~~Figure 5~~. Therefore, the presence of the designed internal hollow sections can not only improve safety under impact, but also maintain similar blast performance.

Table 4 Blast wave pressures and their arrival time at Sensor A and Sensor B

	Sensor A		Sensor B	
	Pressure (MPa)	**Arrival time (μs)**	**Pressure (MPa)**	**Arrival time (μs)**
Solid explosive	55.3	13.3	65.8	16.8
Explosive with small hollow sections (d=5 mm)	55.2	17.2	63.8	19.9
Explosive with large hollow sections (d=5 mm)	56.7	23.7	64.9	25.9

3D Simulations

To further consolidate the investigations carried out under the 2D model, a 3D version is also tested using the same material and EOS data highlighted in Table 2~~Table 2~~. However, the 3D version allows for more freedom in the geometry selected compared to the 2D axisymmetric model, which is limited to helical voids, within the cylindrical geometry. For the testing of the 3D model a 100 mm cube was specified, to establish a benchmark detonation point when impacted by a prescribed 50g blunt projectile made of brass. As previously mentioned, the projectile is based upon EMTAP test 36 standards, but was blunted to increase contact surface area ensuring a larger pressure transfer. In practice, one would expect the bullet design utilised in EMTAP testing to deliver lower contact pressures, and therefore require higher impact speeds to achieve the same detonations.

The set-up was first tested with no infill inclusions as a solid cube of charge, the testing of this model resulted in a Shock to Detonation Threshold (SDT) velocity of 1100 m/s, providing the benchmark for future tests. With this in mind, similar cylindrical voids to the 2D investigations, were introduced to the solid charge. The first trial implemented two rows of ~~6~~ 3 mm in ~~diameter~~ radius cylindrical voids, set 10 mm from the edge of the impact site, displayed within Figure 7~~Figure 7~~. These voids showed an increase in the required detonation speed as expected up to 1430 m/s.

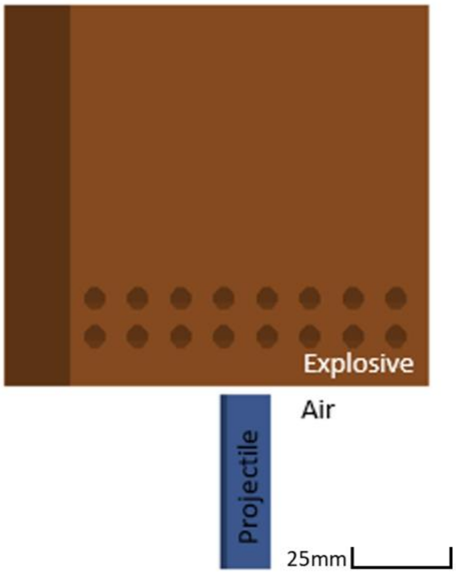

Figure 7 Schematic of an example 3D model. With ~~6~~ 3 mm radius voids 10 mm from impact site.

To establish the effect of the distance of the voids from the impact site, further tests were executed whereby the voids were positioned 14 mm from the impact site, a further 4 mm from the previous trial. The effect of this was significant, with the required detonation speed reducing from the previous void trial of 1430 m/s to 1145 m/s, just a 4.5 % increase on the benchmark SDT of 1100 m/s. To further examine this effect, the voids were moved within 4 mm of the impact site, the impact of this was an increase in the SDT from the solid benchmark of 201.8 % to 2220 m/s.

To examine an additional aspect of the inclusion of voids, the voids were designed to pass through the whole of the charge; this uncapped model saw an inability for the projectile to trigger a full detonation at impact speeds up to 2500 m/s. This is likely a result of venting of the charge due to the voids being unenclosed, preventing the ability for pressure to build up to a critical point to result in the full detonation of the charge. However, the implementation of uncapped voids preventing an impact triggered detonation is also likely to affect the planned detonations and was also proven to be location sensitive, in relation to the impact site. This was shown by locating the voids out of the direct path of the projectile, therefore leaving a mass of solid charge in the immediate impact site. The outcome of this geometrical change was a full detonation being achieved at 1300 m/s, still an improvement on the completely solid charge, but an even more significant reduction than when the voids were appropriately located in the vicinity of the impact site.

When analysing the pressure results from the numerous simulations, while considering the detonated model, the initial pressure built up over the first 10-15 mm region from the impact site, to in excess of 15 GPa. Whereas the non-detonating simulations displayed an initial pressure spike at the impact site before falling away. Figure 9~~Figure 9~~ to Figure 11~~Figure 11~~, display the tracked pressures for a solid charge, with ~~6~~ 3 mm ~~diameter~~ radius voids, 4 mm from the impact site, and ~~6~~ 3 mm ~~diameter~~ radius voids 14 mm from the impact site respectively. All three cases utilising the same impact speed of 1145 m/s to show a direct comparison in resultant pressures. The voids set 4 mm from the impact site display a substantial difference than the other two models, with the pressure clearly dropping after initial impact as the pressure wave is dissipated by the voids. When comparing this to the solid charge which shows a continual build-up in pressure up to the point where the charge begins to detonate at approximately 0.005 ms, which is the cause for the continued pressure rise beyond 16 GPa. In contrast to the graph in Figure 11~~Figure 11~~, for the voids set 14 mm from the impact site, after the initial gain in pressure a drop is observed before a delayed continued raise and detonation occurs. The dip in tracked pressures is due to the pressure concentrations diverging after passing the voids, as illustrated in Figure 8~~Figure 8~~ where the divergence in comparison to the solid charge can be clearly depicted leading to a delay in detonation. With the detonation developing off the direct path of the projectile and the monitored pressures, with the latter stages of the detonation displayed beyond 0.01 ms in Figure 11~~Figure 11~~. This delayed detonation due to the voids, displays continuity in the models with a similar effect noted within the 2D trials.

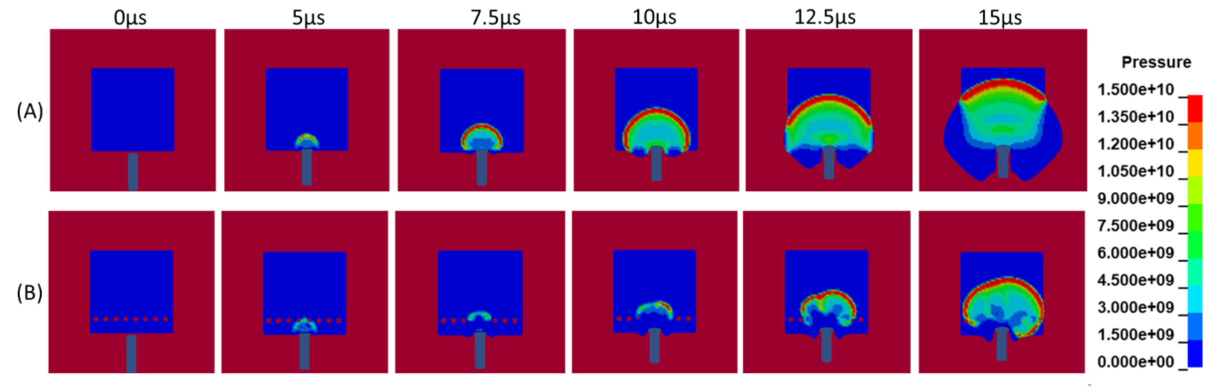

Figure 8 Pressure plot over a series of timesteps. (A) Solid Charge; (B) Charge with voids 14 mm from impact site.

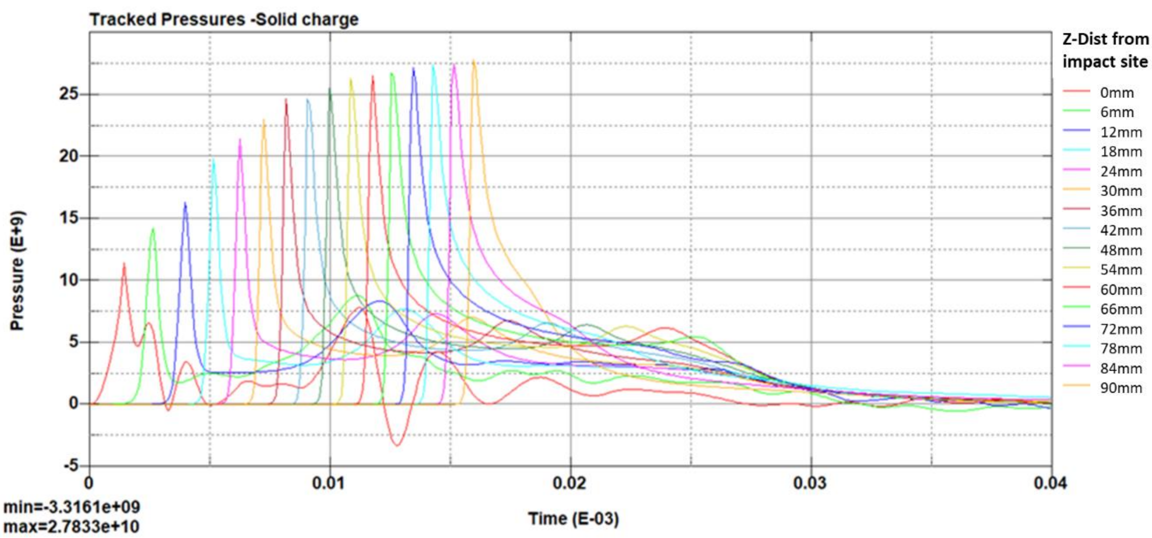

Figure 9 Pressure curve for tracked pressures from impact site to 90 mm from impact site, for solid charge benchmark,1145 m/s impact speed.

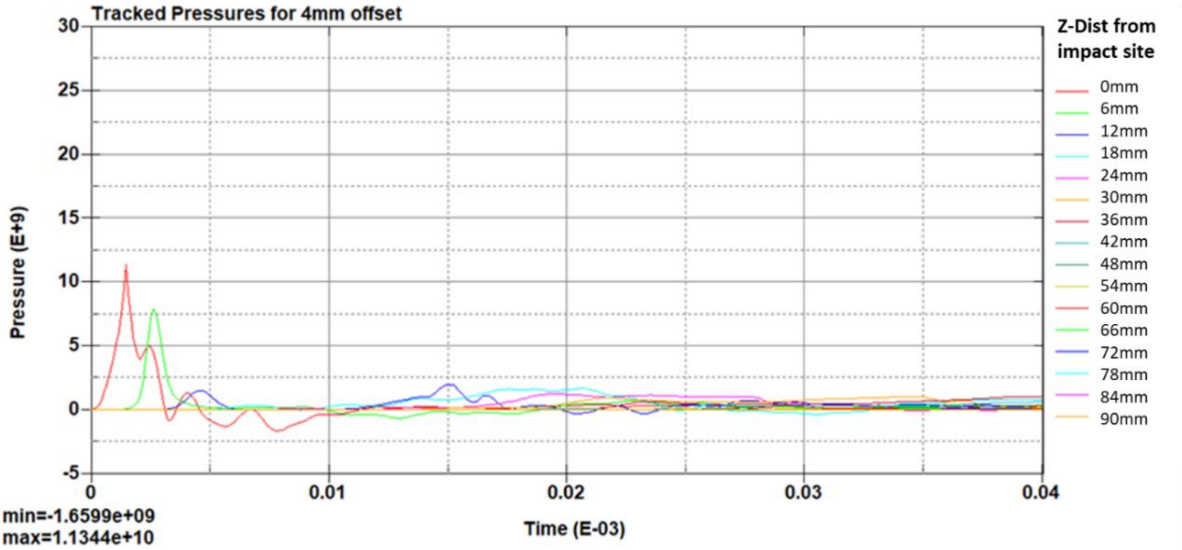

Figure 10 Pressure curve for tracked pressures from impact site to 90 mm from impact site, for ~~6~~ 3 mm radius voids located 4 mm from impact site, 1145 m/s impact speed.

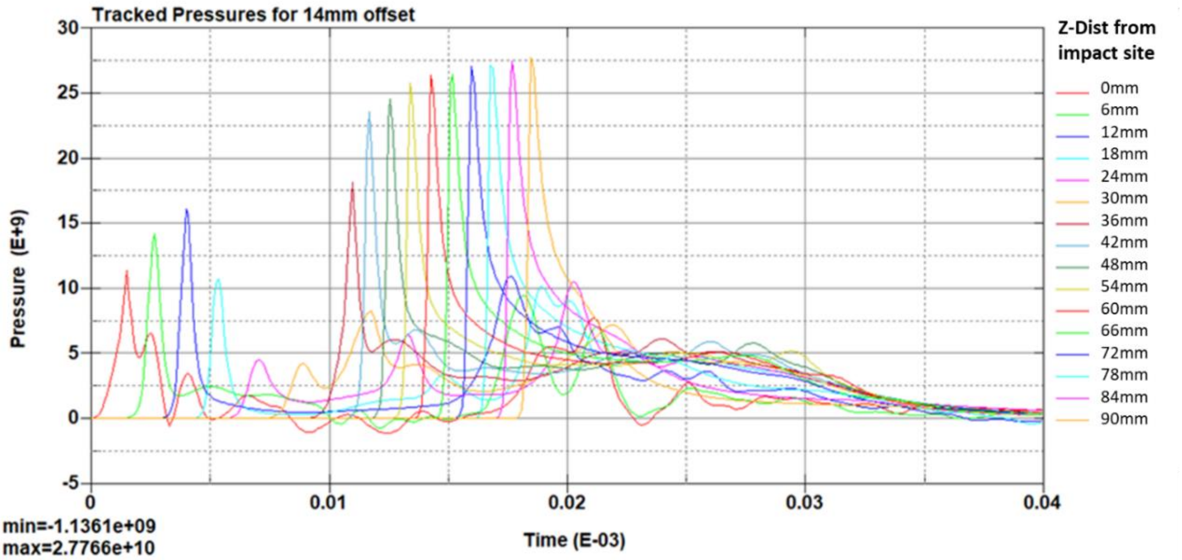

Figure 11 Pressure curve for tracked pressures from impact site to 90 mm from impact site, for ~~6~~ 3 mm radius voids located 14 mm from impact site, 1145 m/s impact speed.

To aid the understanding of the performance of current standard ALM infill patterns, and their impact upon the reactivity of the charges. A basic infill pattern provided in Figure 12~~Figure 12~~ was set up within the same 100 mm cube, which displayed issues of venting causing excessively large impact speeds to be required up to 2500 m/s. Whilst this may appear beneficial in preventing detonation from impact, the venting can lead to charges failing to fully detonate even under a planned ignition. Therefore, tests were also carried out ensuring the infill was fully enclosed to eliminate the effects of venting, which had previously been observed to prevent the charge passing from deflagration to detonation (DDT). The difference in the burn fraction as a result of this change can be seen in Figure 13~~Figure 13~~.

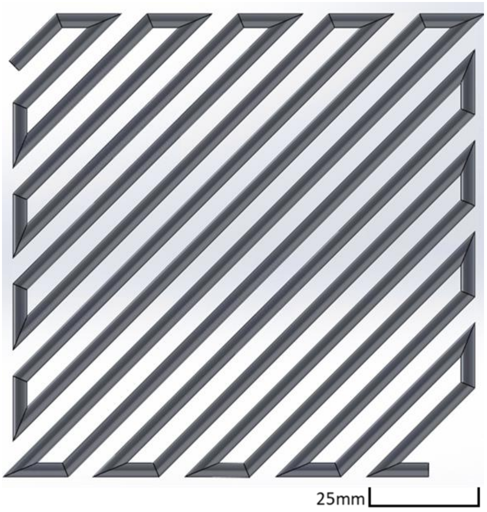

Figure 12 Cross section of the infill pattern utilised for infill simulation.

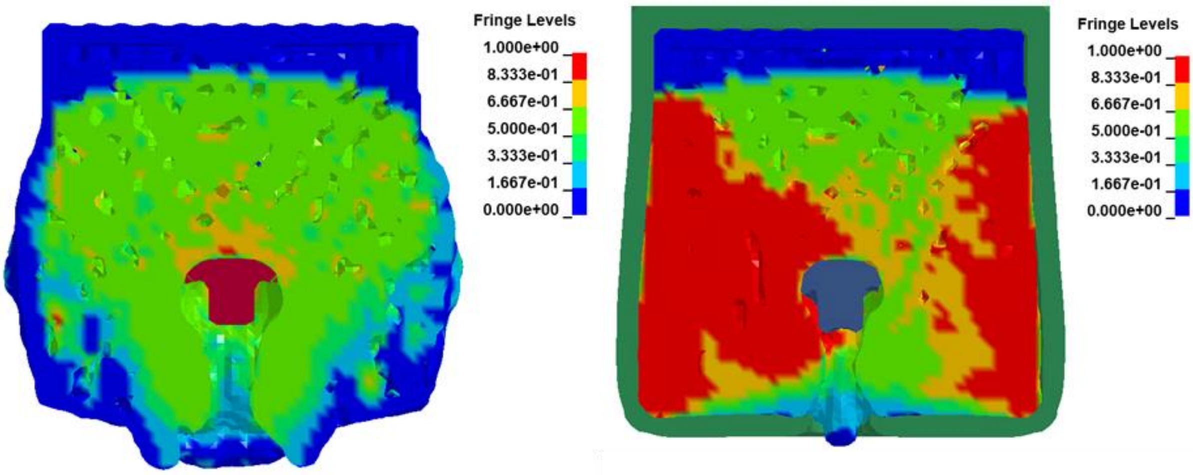

Figure 13 Comparison of burn fraction from standard infill of an unenclosed charge (left) and one encased with 5 mm steel casing (right).

A summary of the key tested models are gathered in Table 5~~Table 5~~, highlighting the percentage increase in SDT and the volume of charge sacrificed to achieve this. Trying to maintain the maximum volume of charge is key for planned detonations. From the table the conventional infill patterns do not offer the best gain in SDT, when considering the volume of charge sacrificed to obtain this improvement; particularly when comparing to the ~~6~~ 3 mm ~~diameter~~radius, 4 mm offset example. However, the infill pattern does offer impact protection on each face of the cube, so applying the ~~6~~ 3 mm ~~diameter~~ radius void design to each face to offer this same level of protection, would lead to an energetic volume sacrifice of 26.4%, compared to the infill's 43%.

Table 5 Summary of key tests, volume of charge lost, and SDT improvements.

Model	% Volume of energetic material sacrificed.	SDT Velocity	% Difference in SDT
Solid Charge	0 %	1100 m/s	-
3 mm radius voids- 4 mm offset	4.4 %	2220 m/s	+101.8 %
3 mm radius voids- 10 mm offset	4.4 %	1430 m/s	+30.0 %
3 mm radius voids- 14 mm offset	4.4 %	1145 m/s	+4.5 %
Standard Infill Pattern	43 %	~~<~~>2500 m/s	~~<~~>127.3 %
Standard Infill Pattern - encased	43 %	2170 m/s	+97.3 %

From the 2D and 3D investigations, an improved understanding of the effects of voids and the importance of size and location has been made. This research has identified two main factors to securely design: the size of the internal voids, and their locations relative to the impact site. These two factors provide concise information, with the larger voids clearly seen in Table 3~~Table 3~~ to increase the SDT of the charge, whilst the distance of the void from the impact site also having a significant effect upon the SDT of the charge.

The reasoning behind the two attributes of void size and location are based upon the pressure build up within the charge around the impact site. The solid charge allows for the pressure to build up to a point that causes the detonation within the charge; once a large enough portion of the charge has reached this point; the full detonation will likely occur, bypassing any voids or internal features, providing they do not offer venting. Therefore, the distance from the impact site is key, as when a significant region of solid charge is within the impact site this will allow for DDT to occur, consequently triggering the detonation of the HE. The voids themselves act as a way of distributing pressure and energy from the impact, with the larger voids offering a more substantial region of air to absorb the pressure and energy. This effect is supported by the highlighted and known effects of venting, whereby the charge has a means of syphoning off the increased pressure and energy to the surrounding environment, preventing a detonation.

Considering these factors, it can be concluded that the location of the voids is the most critical factor, as a well-designed void located away from the impact site will be ineffective. As such voids located far beyond the surface of the charge will be redundant and reduce the overall charge's volume for limited benefit. This means that conventional infill patterns which pass through the whole of the geometry are not the most efficient means of increasing the SDT point of a HE.

From this information, the design required should aim to absorb and distribute the impact pressures to a non-detonation triggering limit. Whilst trying to maintain uniformity for the whole charge, to provide protection against impact from all angles. As in real life events the impact site will not be known. Therefore, an air-cushion design was proposed whereby a large void will be located 5 mm from the surface of the charge to ensure sufficient rigidity in the outer surface of charge, as shown in Figure 14~~Figure 14~~. The internal portion of the charge requires supporting and connecting to the outer face of the geometry. In turn resulting in certain small regions of the design, with a solid charge path from the outer face to the inner charge volume, where the designed voids will not be as effective. However, this problem applies to all designs where the need for supports within the geometry will lead to certain areas where the implemented voids cannot be as effective.

The simplicity of this design is intended to offer a large area of energy absorption whilst removing as little of the charge as possible, in this instance 22 % of the charge volume is sacrificed.

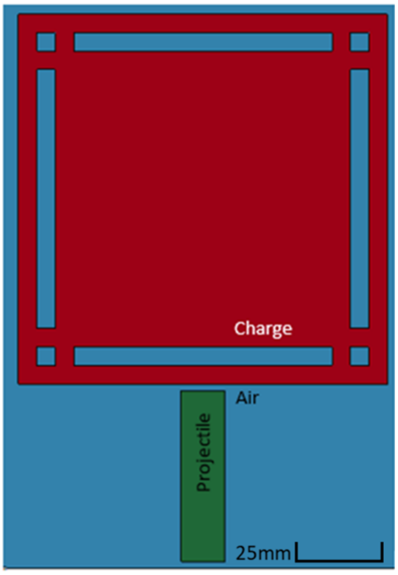

Figure 14 Cross sectional view of proposed air cushion design.

The design was tested utilising the same previously used method, whereby it was seen to be very effective at increasing the SDT of the HE, with the design offering a 79.5 % increase in SDT from 1100 m/s up to 1975 m/s at the expense of 22 % of the charge volume. Offering a strong relationship for safety advantage against loss of charge.

The design itself may be more easily manufactured with the use of an inert material within the voids. However, based on the previous tests this is believed to not be as effective as the inert material will not be able to dissipate the pressure and absorb the energy of the impact as well as air. To prove this hypothesis the air was substituted for a silicone rubber inert material; this change resulted in a significant drop in the required impact speed from the air version, with a speed of 1630 m/s triggering the detonation. However, this still offers over a 48.2 % improvement, it is not seen to be as effective as air, due to the rubber's ability to transfer more pressure and energy. This is illustrated in Figure 15~~Figure 15~~, showing the tracked pressures over the first 21 mm from the impact site, with the points at 5, 7, and 9 mm being set within the void region of the charge. The pressure is seen to drop off quicker after entering the air void, with the pressure failing to rebuild after this and trigger the detonation. Whereas the inert material, whilst decreasing the pressure, still allows sufficient transfer of pressure for the detonation to be triggered. The drop-off then observed between 0.005 ms and 0.008 ms is due to the detonation and continued build of pressure propagating further from the impact site, before dispersing back to the centre line of the charge and the location of the tracked points, during the later stages of detonation.

If a multi material ALM printer was utilised, this would allow for the improved benefits of the inert material over the energetic material, to be used to generate the supports around the air cushion, which would lead to a safety improvement for 100 % of the surface of the charge.

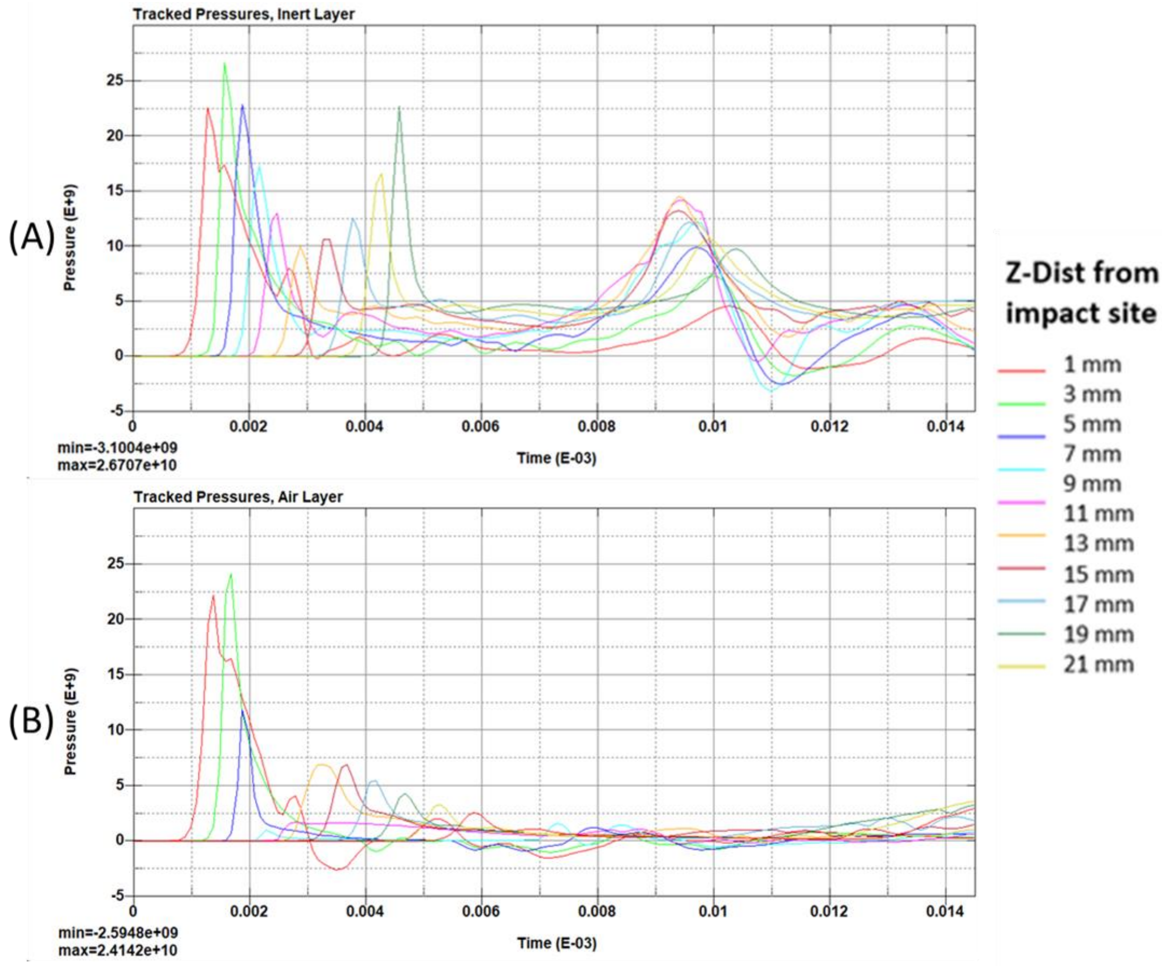

Figure 15 (A) Pressure curve for tracked pressures for first the 21 mm from impact site for inert cushion, 1630 m/s impact speed. (B) Pressure curve for tracked pressures for the first 21 mm from impact site for air cushion, 1630 m/s impact speed.

Conclusion

The proposed research has identified that the inclusion of voids within a HE can alter the shock to detonation threshold significantly. This in turn offers the chance to improve the safety of charges against unplanned impact detonations. With the key focus of void inclusions being to absorb energy and distribute pressure. For this aim, it was found the two key considerations for the void geometry being employed was the size and location relative to impact site.

In order to ensure 360-degree protection, one proposed design offers a 79.5 % improvement in required shock to detonation velocity, compared to a conventional solid charge, whilst only sacrificing 22 % of the volume. This principle of utilising voids to absorb energy from impact can be easily applied to all conventional charge geometries, through the use of additive layer manufacturing and suitably adapted to match the users' needs.

Acknowledgement

The ASTUTE 2020 (Advanced Sustainable Manufacturing Technologies) operation, supporting manufacturing companies across Wales, has been part-funded by the European Regional Development Fund through the Welsh Government and the participating Higher Education Institutions. This project was also supported by the EPSRC Impact Acceleration Account. The Authors would like also to express their great appreciation to the local collaborative company for the supports.

References

1. *National Park Service handbook for the storage, transportation, and use of explosives*. 1999, Washington, DC: U.S. Dept. of the Interior, National Park Service].
2. Makwana, D.R. and K. Laxminarayan, *Numerical Simulation of an Armoured Vehicle to Anti – Vehicle Mine Blast to Optimize the Structural Rigidity*, in *2011 Americas Hyperworks Technology Conference (HTC 2011)*. 2011: Orlando, Florida (United States). p. 1-7.
3. Rasico, J.G., C.A. Newman, and M.R. Jensen, *Modelling fragmentation of a 155 mm artillery shell IED in a buried mine blast event.* International Journal of Vehicle Performance, 2018. **4**: p. 323-346.
4. Zhou, X., Y. Mao, D. Zheng, L. Zhong, R. Wang, B. Gao, and D. Wang, *3D printing of RDX-based aluminized high explosives with gradient structure, significantly altering the critical dimensions.* Journal of Materials Science, 2021. **56**(15): p. 9171-9182.
5. Mueller, A.H., *The Little Things that Matter: Detonation Manipulation through Sub-Critical Diameter Structure in High Explosives*. 2019, Los Alamos National Lab.(LANL), Los Alamos, NM (United States). LA-UR-19-22910.

6. Ma, S., X. Zhang, Y. Lian, and X. Zhou, *Simulation of high explosive explosion using adaptive material point method.* CMES - Computer Modeling in Engineering and Sciences, 2009. **39**: p. 101-123.
7. Li , S. and W.K. Liu *Meshfree and particle methods and their applications.* Applied Mechanics Reviews, 2002. **55**(1): p. 1-34.
8. Slavik, T.P., *A coupling of empirical explosive blast loads to ALE air domains in LS-DYNA®*, in *9th World Congress on Computational Mechanics, IOP Conference Series: Materials Science and Engineering 10*. 2010, IOP Publishing Ltd: Sydney, Australia. p. 012146.
9. Randers-Pehrson, G. and K.A. Bannister, *Airblast Loading Model for DYNA2D and DYNA3D.* Army Research Laboratory, 1997. **ARL-TR-1310**.
10. Artero-Guerrero, J., J. Pernas-Sánchez, and F. Teixeira-Dias, *Blast wave dynamics: The influence of the shape of the explosive.* Journal of Hazardous Materials, 2017. **331**: p. 189-199.
11. Tabatabaei, Z.S. and J.S. Volz, *A comparison between three different blast methods in LS-DYNA: LBE, MM-ALE, Coupling of LBE and MM-ALE*, in *12th International LS-DYNA Users Conference*. 2012: Detroit, United States. p. 1-10.
12. Huang, Y., M.R. Willford, and L.E. Schwer, *Validation of LS-DYNA® MMALE with blast experiments*, in *12th International LS-DYNA Users Conference*. 2012: Detroit, United States. p. 1-12.
13. Alia, A. and M. Souli, *High explosive simulation using multi-material formulations.* Applied Thermal Engineering, 2006. **26**(10): p. 1032-1042.
14. Benson, D.J., *A mixture theory for contact in multi-material Eulerian formulations.* Computer methods in applied mechanics and engineering, 1997. **140**(1-2): p. 59-86.
15. Lee, E.L., H.C. Hornig, and J.W. Kury, *Adiabatic Expansion Of High Explosive Detonation Products*. 1968: Lawrence Radiation Laboratory at University of California, Livermore, CA (United States). UCRL-50422.
16. Lee, E.L. and C.M. Tarver, *Phenomenological model of shock initiation in heterogeneous explosives.* The Physics of Fluids, 1980. **23**(12): p. 2362-2372.
17. Tarver, C.M., *Modeling Detonation Experiments on Triaminotrinitrobenzene (TATB)-Based Explosives LX-17, PBX 9502, and Ultrafine TATB.* Journal of Energetic Materials, 2012. **30**(3): p. 220-251.
18. White, B.W. and C.M. Tarver, *Ignition and growth modeling of detonation reaction zone experiments on single crystals of PETN and HMX.* AIP Conference Proceedings, 2017. **1793**(1): p. 030001.
19. Tarver, C.M., *Ignition and growth reactive flow modeling of detonating LX-04 using recent and older experimental data.* AIP Conference Proceedings, 2018. **1979**(1): p. 100042.
20. Miller, P.J. and G.T. Sutherland, *Reaction rate modeling of PBXN-110.* AIP Conference Proceedings, 1996. **370**(1): p. 413-416.
21. *LS-DYNA*. [cited 2022; Available from: https://www.lstc.com/products/ls-dyna.
22. Schwer, L.E., *Impact and Detonation of COMP-B: An Example using the LS-DYNA EOS: Ignition and Growth of Reaction in High Explosives*, in *12th International LS-DYNA Conference*. 2012: Detroit, United States. p. 1-20.